Journal of Catalysis 286 (2012) 237–247

Contents lists available at SciVerse ScienceDirect

Journal of Catalysis

journal homepage: www.elsevier.com/locate/jcat

A new view on the relations between tungsten and vanadium in V_2O_5—WO_3/TiO_2 catalysts for the selective reduction of NO with NH_3

Patrick G.W.A. Kompio [a], Angelika Brückner [b], Frank Hipler [c], Gerhard Auer [c], Elke Löffler [a], Wolfgang Grünert [a,*]

[a] Lehrstuhl für Technische Chemie, Ruhr-Universität Bochum, Bochum, Germany
[b] Leibniz Institute for Catalysis at Rostock University, Rostock, Germany
[c] Crenox GmbH, Krefeld, Germany

ARTICLE INFO

Article history:
Received 25 August 2011
Revised 7 November 2011
Accepted 9 November 2011
Available online 10 December 2011

Keywords:
Selective catalytic reduction
Ammonia
V_2O_5
WO_3 promotor
TiO_2
EPR
Temperature-programmed reduction

ABSTRACT

The relation between tungsten and vanadium oxide species in V_2O_5—WO_3/TiO_2 catalysts for the selective catalytic reduction of nitrogen oxides by ammonia was studied with two series of catalysts containing 0.5–5 wt.% V_2O_5 and 0 or 10 wt.% WO_3 impregnated onto a high surface-area titania hydrate of anatase structure to keep theoretical surface coverages of the transition metal oxides $\leqslant$1. The catalysts, which were investigated by XRD, nitrogen physisorption, Raman and EPR spectroscopy, temperature-programmed reduction (TPR), and catalytic reduction studies, all exhibited the well-known acceleration of the SCR reaction by the tungsten promoter. From the EPR spectra and the TPR profiles, it was concluded that the presence of tungsten induces the formation of a surface oxide phase with intimate mixing between vanadium and tungsten oxide species instead of pronounced surface vanadium oxide island formation, which was found in the absence of tungsten. This suggests that the promotional effect of tungsten may originate from a direct influence on the neighboring vanadium oxide species or from the disruption of too large surface vanadium oxide ensembles.

1. Introduction

Selective catalytic reduction (SCR) is a well-established technology for the removal of harmful nitrogen oxides (NO_x) from stationary emission sources [1]. The ammonia reductant reduces NO_x selectively to nitrogen (e.g., for NO):

$$4NO + 4NH_3 + O_2 \rightarrow 4N_2 + 6H_2O$$

Typical industrial catalysts contain V_2O_5 and WO_3 supported on TiO_2 (anatase) [1]. Vanadium oxide is the active component, but due to its toxicity and its activity for undesired SO_2 oxidation, its content is usually $\leqslant$2 wt.% [2,3]. WO_3 is a promoter and stabilizer [4,5], typically with an amount of 10 wt.%, which is described to increase the activity, widen the temperature range in which the catalysts are selective and to stabilize their physical surface area [2,4,6,7]. These catalysts, which provide high NO_x conversion and N_2 selectivity between 550 and 670 K [1,8], are often considered to be technically mature and well studied. There are, however, competing views on the origin of the promoting effect of the W component.

It has long been known that the interaction of TiO_2 with supported V(V) or W(VI) oxide species leads to surface oxide phases with structures strongly different from those of the corresponding bulk oxides [9,10]. In the case of vanadium, isolated surface oxide species with a strongly distorted tetrahedral geometry were observed in dehydrated samples at low V oxide coverage [10–15]. With increasing loading, two-dimensional islands of oligomeric or polymeric metavanadate species are formed [9–11,14], and crystalline V_2O_5 nanoparticles were observed at high vanadium content [11,14]. There was a dispute if aggregates or oxide crystals may occur at V oxide contents below the theoretical monolayer coverage, but it was shown by surface analytical techniques that in well-prepared catalysts, the surface oxide species do not grow into the third dimension until the support is completely covered by the two-dimensional surface oxide phase [16,17]. In dehydrated WO_3/TiO_2 catalysts, strongly distorted octahedral surface species ($(—O)_5$—W=O) were reported to predominate up to high tungsten oxide coverage [11]. They were found to coexist with tetrahedral monovanadate and polymeric surface vanadates in V_2O_5—WO_3/TiO_2 catalysts: The abundance of the polymeric species increased with increasing tungsten content at metal coverages which considerably exceeded the monolayer limit if both metals were to compete for the same surface sites [11].

There is remarkable agreement regarding the nature of the active sites for ammonia-SCR in V_2O_5/TiO_2. Although isolated

* Corresponding author. Address: Lehrstuhl für Technische Chemie, Ruhr-Universität Bochum, P.O. Box 102148, D-44780 Bochum, Germany. Fax: +49 234 321 4115.
E-mail address: w.gruenert@techem.rub.de (W. Grünert).

0021-9517/$ - see front matter © 2011 Elsevier Inc. All rights reserved.
doi:10.1016/j.jcat.2011.11.008

vanadium oxo sites were proposed in early studies [18], the particular role of oxo-bridged dimeric vanadium sites has been emphasized by many groups [19–23]. A stronger than proportional increase of the catalytic activity with the vanadium content [22,24] indeed supports the higher activity of dimeric (polymeric) sites, but also indicates an activity of isolated V oxo centers. The latter have been suggested to be an order of magnitude less active but more selective for N_2 formation [24]. Brønsted sites (V—OH) have been found to be involved in the reaction as well [25–27]. The observations made with V_2O_5/TiO_2 catalysts are well explained by a catalytic cycle proposed by Topsoe et al. [28–31] on the basis of *in situ* FT-IR and online mass spectrometric studies, which employs dimeric sites comprising both a V—OH and a V=O entity.

Previous explanations for the promoting effect of the W component in these catalysts rely on various experimental observations. Thus, their acidity was increased in the presence of tungsten, which favors the ammonia supply for the reaction [6,32]. Tungsten oxide was reported to delay the loss of BET surface area [5,33] and the transformation from monomeric vanadyl to crystalline V_2O_5 during aging [34]. It was also observed to increase the reducibility of the V component [6], which might favor the catalytic reaction. The aspect most closely related to the above-mentioned concept of the active sites was, however, the suggestion that the W component occupying a significant part of the support surface enforces a closer proximity on the surface V oxide species encouraging thus the formation of the most active V—O—V structures [6]. In the latter role, the tungsten species are just spectators. One might, therefore, expect that similar activities can be achieved also in absence of tungsten by systematically decreasing the TiO_2 surface area, but reports on such an approach are not available.

We have now studied the influence of tungsten on V_2O_5/TiO_2 catalysts for NH_3-SCR by comparing two series of catalysts with identical vanadium contents differing by the presence or absence of 10 wt.% WO_3. The catalysts were prepared by a method near to industrial practice (incipient wetness impregnation). Deliberately mild conditions were, however, chosen for the final thermal step (synthetic air, 623 K, 1 h), because we did not aim at maximum activity, instead the purpose was to fix the species structure resulting from the impregnation by inducing condensation with the support OH groups. The promotional effect of the tungsten was verified by catalytic investigation of the SCR activity, and the structural properties of the samples were studied by XRD, nitrogen physisorption, temperature-programmed reduction, EPR, and Raman spectroscopy. The data suggest that vanadium and tungsten oxide species tend to create a mixed surface oxide phase and that the effect of tungsten is rather to prevent than to encourage island formation of the surface V oxide component.

2. Experimental

2.1. Materials

Samples were prepared starting from a titania hydrate in the anatase modification, for which an ignition loss of 11.9%, a specific surface area of >250 m^2/g, a density of 3.8 g/cm^3, a sulfate content of $\leqslant$2%, and impurity contents of Fe_2O_3 and Na_2O <100 ppm each are specified by the manufacturer. Sources for W and V were ammonium para tungstate (APT, $(NH_4)_{10}(H_2W_{12}O_{42})\cdot 4H_2O$, Tima Tungsten GmbH, impurity elements <0.0088 wt.%) and ammonium meta vanadate (NH_4VO_3, Acros, 99%). The reaction feed was prepared from pre-mixed gas mixtures (Air Liquide).

2.2. Catalyst preparation and characterization

WO_3 was deposited on the TiO_2 hydrate by wet impregnation of APT from its aqueous solution, the concentration of which was chosen to obtain a tungsten oxide loading of 10.0 wt.%. Subsequently, the material was dried at 383 K overnight and calcined at 713 K for 1 h (heating ramp 2 K/min to 400 K, then 5 K/min, in flowing synthetic air, 20% O_2/He), which brought the BET surface area down to 140 m^2/g.

The WO_3/TiO_2 material and the initial TiO_2 hydrate were wet impregnated with an aqueous NH_4VO_3 solution to obtain loadings of 0.5, 1.5, 3.0, and 5.0 wt.% V_2O_5. The eight resulting catalysts were dried overnight at 383 K and calcined in O_2/He (20% O_2, synthetic air) at 623 K for 1 h, which will be denoted as "reference calcination". These materials will be labeled $W_{10}V_x$ and V_x, respectively, where x reports the V_2O_5 content (wt%). For reference purposes, one V_2O_5/TiO_2 catalyst (5 wt.% V_2O_5) was made with a BET surface area similar to those of the tungsten-containing catalysts (cf. Section 3.1.) by employing the TiO_2 hydrate after a calcination at 673 K for 1 h resulting in a BET surface area of 128 m^2/g ($\rightarrow V^*_{5.0}$).

Specific surface areas of the catalysts were determined by nitrogen physisorption using a Quantachrome Autosorb-1 MP instrument. Prior to analysis, the samples were outgassed for 2 h at 573 K. The XRD measurements were performed with a D8 Advance instrument (Bruker AXS), using Cu Kα radiation (0.15413 nm, 40 kV, 40 mA). Temperature-programmed reduction was made with 4.5% H_2 in Ar, ramping the temperature to 1073 K or 1273 K at 10 K min^{-1}. The effluent gas was analyzed by a Hydros thermal conductivity detector (Fisher-Rosemount).

The EPR spectra of dehydrated samples (1 h at 623 K in Ar) were measured with an ELEXSYS 500–10/12 CW spectrometer (Bruker) using a microwave frequency of 9.5 GHz (X band), a power of 6.3 mW, a modulation frequency of 100 kHz, and a modulation amplitude of 0.5 mT. Spectra were recorded at 77 K. Spectral intensities were normalized on the sample mass. Therefore, intensities are directly comparable, although an integration was not performed. The simulation of the EPR spectra was done by the program SIM14S [35] (version 06/09/1991).

FT-Raman spectra of dehydrated samples (1 h at 623 K in Ar) were measured with a Thermo Nicolet Vectra Plus Instrument using a laser wavelength of 1064 nm (NIR) at 370 mW. The spectrometer resolution was 4 cm^{-1}. The resultant interferograms were collected with a liquid nitrogen-cooled Ge detector; the spectra were visualized with the OMNIC 6.2 software. Some spectra (see legend to Fig. 7b) were measured with a DRX Raman Microscope (Thermo Scientific).

2.3. Catalytic measurements

The catalysts were pressed and sieved to arrive at a grain size of 250–350 μm. Their activity was studied in a micro flow reactor (inner diameter – 4.2 mm) with a feed gas mixture containing 1000 ppm NO, 1000 ppm NH_3, and 2% O_2 in He. The experiments were made with a modified residence time W/F of 3.3×10^{-3} g s ml^{-1} (catalyst mass – 10 mg, feed flow – 183.3 ml min^{-1}). With an approximate bed density of 0.68 g cm^{-3} deduced from the bed height obtained, this results in a GHSV of $\approx$750,000 h^{-1}. In the experiments, the temperature was raised to the reaction temperatures at 5 K min^{-1} and conversions were recorded after the steady state had been attained. Data obtained between 423 and 723 K will be reported in this paper, although the conversions achieved above the calcination temperature of 623 K cannot be referred to the initial state of the catalysts.

NO and NH_3 conversions were determined with a non-dispersive IR photometer (XStream, Emerson). An NO_2 analyzer in the analytical scheme did not indicate formation of sizable amounts

of NO_2. In these experiments, N_2O was not analyzed. However, in similar experiments with a different series of V_2O_5—WO_3/TiO_2 catalysts [36,37], the nitrogen selectivity remained typically >95% below 723 K.

3. Results

3.1. Texture studies

In Table 1, the BET surface areas of the catalysts and the titania hydrate, all after the reference calcination (623 K, 1 h), are summarized and employed for the evaluation of transition metal surface coverage data. The surface areas of the tungsten-containing catalysts are between 115 and 125 m^2/g, those of the tungsten-free samples between 175 and 225 m^2/g. Unexpectedly, there is no inverse relation between BET surface area and vanadium content, although surface vanadium oxide species have been described to destabilize the texture of TiO_2. A parallel trend can be noted in both series, although the changes between the W-containing catalysts seem to be near the limits of experimental error. However, it seems significant that the lowest BET surface area occurs with 1.5 wt.% V_2O_5, for reasons which have not been understood so far. It is also remarkable that the BET surface area of all tungsten-containing catalysts fell short of 140 m^2/g, although the final calcination temperature (623 K) was well below that employed to establish the 140 m^2/g of the WO_3/TiO_2 precursor.

Table 1 indicates a failure in our initial intention to keep the BET surface areas of both series in a comparable range. This means that indeed two parameters are changed between these two series: the presence of tungsten and the BET surface area. It will be seen below, however, that this drawback will not interfere with the conclusions to be drawn from the data. Sample $V^*_{5.0}$ with a BET surface area comparable to that of the W-containing catalysts has been included in the study to remove remaining doubt.

For the evaluation of the theoretical surface coverage of the transition metal oxide species, different parameters for their areal monolayer density are available in the literature: according to [38], 12.7 μmol V or 6.8 μmol W can be accommodated per m^2 support surface; according to [39], the densities are somewhat less (10.4 μmol V or 4.6 μmol W per m^2). In Table 1, coverage degrees according to both sets of density data are given. For the tungsten-containing catalysts, the coverage can be differentiated with the W/V atomic ratios reported in the last column. It can be seen that the V-only catalysts are very dilute whereas in the tungsten-containing samples the TiO_2 appears to be largely covered by the supported species, in particular at the higher vanadium oxide contents.

In Fig. 1, XRD patterns of some catalysts are compared with that of the titania hydrate, after the reference calcination. The diffractograms are dominated by the reflections of anatase, their considerable width indicates a small primary particle size, which may be evaluated by the Scherrer equation. Particle sizes may be also estimated from the BET surface areas (Table 1) via $d_{BET} = 6/(\rho S_{BET})$, where ρ is the material density. For the titania hydrate, the BET surface area provides a much smaller particle size than XRD ($d_{BET} \approx 6$ nm, $d_{XRD} = 11.8$ nm, from the (101) reflection). This suggests a strong surface roughness of the particles, a crystalline core being probably surrounded by an amorphous, porous overlayer. With the loss of surface area due to the influence of the impregnated vanadium, the discrepancy decreased somewhat: for $V_{5.0}$ the corresponding diameters were $d_{BET} \approx 7.5$ nm and $d_{XRD} = 11.4$ nm. The best coincidence was obtained with the tungsten-containing samples, which had experienced the intermediate calcination at 713 K. Here, the BET-derived sizes (13.7, 12.9, and 14.2 nm for $W_{10}V_{1.5}$, $W_{10}V_{5.0}$, and $V^*_{5.0}$) compare well with 14.1, 12.2, and 15.0 nm obtained from the diffractograms.

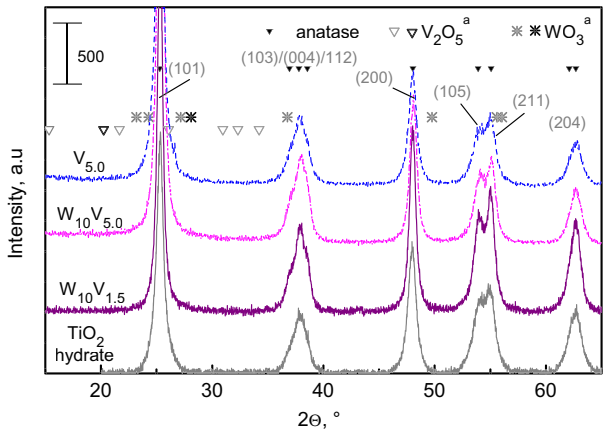

Fig. 1. XRD patterns of tungsten-free and tungsten-containing V_2O_5/TiO_2 catalysts and of the titania hydrate precursor after the reference calcination (623 K, 1 h). [a]Expected reflections of V_2O_5 (▽) and WO_3 (✳), main reflections in black.

For all catalysts, the presence of crystalline WO_3 and V_2O_5 can be excluded on the basis of the diffractograms (Fig. 1) even in samples where the theoretical surface coverage degree of the transition metal oxides is near or above 1 (cf. Table 1). There is a tiny hump at $2\Theta = 26.65$ ° in the diffractogram of $V_{5.0}$, which is near to reflections expected for WO_3 and V_2O_5. The latter are, however, minor signals in the reflection patterns of the oxides, and the more prominent signals are missing. Apparently, the peak arises from minor amounts of quartz present in the sample analyzed ((101) reflection at 26.64°). There was not any V_2O_5 signal in the XRD pattern of $V^*_{5.0}$ either (not shown).

3.2. Catalytic properties

The catalytic activities of our catalysts are summarized in Fig. 2 where the temperature dependence of NO and NH_3 conversions are shown and the temperature range above the calcination temperature has been shaded. The promotion effect of tungsten is clearly visible: at all vanadium contents, the conversion curve of the tungsten-containing samples rises at lower temperature. The ammonia oxidation tendency was very low in all cases. From the curves in Fig. 2a through *d*, it is also obvious that the SCR activity increases with the vanadium content both in presence and absence of tungsten. One may be tempted to examine the relation between activity and vanadium content from these data to confirm the more than proportional relation between them reported in [22,24]. We have attempted this despite the fact that for all suitable temperatures the conversions range from extremely small, not very accurate values till far outside the differential range. Treating the integral

Table 1
Comparison of BET surface areas, transition metal coverages, and W/V atomic ratios.

	BET surface area, $m^2\ g^{-1}$	Surface coverage of transition metal ions, Θ, according to		Atomic W/V ratio
		[38]	[39]	
Titania hydrate	257	0	0	0
$V_{0.5}$	192	0.02_5	0.03	0
$V_{1.5}$	174	0.07	0.09	0
$V_{3.0}$	226	0.11	0.14	0
$V_{5.0}$	212	0.20	0.25	0
$V^*_{5.0}$	111	0.39	0.48	0
$W_{10}V_{0.5}$	119	0.57	0.83	7.8
$W_{10}V_{1.5}$	115	0.66	0.95	2.6
$W_{10}V_{3.0}$	123	0.73	1.02	1.3
$W_{10}V_{5.0}$	122	0.87	1.20	0.8

data with an assumed first-order rate law, we indeed confirmed the expected more than proportional relation except for data points too close to the conversion maxima (e.g. in Fig. 2d), but due to the problems mentioned above this result should not be overemphasized.

Remarkably, the promotion effect is very pronounced just at 5 wt.% V_2O_5 where a theoretical surface vanadium oxide coverage of 20–25% should give rise to abundant V—O—V pair formation already without promotion by tungsten.

3.3. Structural characterization of the vanadium phase

3.3.1. EPR spectroscopy

The EPR spectra of tungsten-free samples and tungsten-containing samples, all measured at 77 K, are compared in Fig. 3 on the same intensity scale. Examples for the spectral simulation are given in Fig. 4. The g and A values resulting from the simulation and the relative intensities I_{rel} (related to the intensity of one of the hyperfine structure (hfs) signals) are summarized in Tables 2 and 3. These tables report also the parameter $\Delta g_{||}/\Delta g_{\perp}$ (with $\Delta g_{||} = g_{||} - g_e$, $\Delta g_{\perp} = g_{\perp} - g_e$; $g_e = 2.0023$ for the free electron), which measures the axial distortion of the V^{4+} center [40,41], and the in-plane delocalization coefficient β_2^{*2} [41], which is a measure of the extent to which the single electron is delocalized toward the O ligands in the equatorial plane of the $O_4V{=}O$ site, i.e., for the degree of covalence of the V—O bonds. β_2^{*2} was obtained from Eq. (1), where the element-specific parameter P, which covers the relation between Bohr magneton μ_b and nuclear magneton μ_N, was set to 184.5 G for a free V^{4+} ion [42]. $\beta_2^{*2} = 1$ means total localization of the unpaired electron at the vanadium nucleus.

$$\beta_2^{*2} = \frac{7}{6}\Delta g_{||} - \frac{5}{12}\Delta g_{\perp} - \frac{7}{6}\left[\frac{(A_{||} - A_{\perp})}{P}\right] \quad (1)$$

The tungsten-free samples were dominated by a broad isotropic singlet which is due to the clustered V—O—V species (Fig. 3a) and increased with increasing vanadium loading. In addition, a hyperfine structure signal typical of an isolated VO^{2+} species can be observed in all samples. In presence of tungsten, the isotropic singlet can be also discerned (Fig. 3b), but it is much less intense than in the tungsten-free catalysts. Instead, the signals of the isolated VO^{2+} species are more complicated, which suggests the presence of at least two different sites. From the spectra, it should be expected that the intensity ratio between the isotropic signal and those of the isolated sites is much larger in the absence of tungsten.

These spectra have been simulated to derive the spectral parameters and relative intensity of signals. Apart from signals of isolated and clustered V^{4+} species, a signal for an O_2^- species was included in the case of tungsten-containing catalysts. Such species had been observed on the bare TiO_2 support and, with enhanced intensity, on the WO_3/TiO_2 precursor [36]. Notably, no tungsten-derived signals could be found on WO_3/TiO_2 [36], therefore such signals were not included in the analysis of the V_2O_5—WO_3/TiO_2 catalysts.

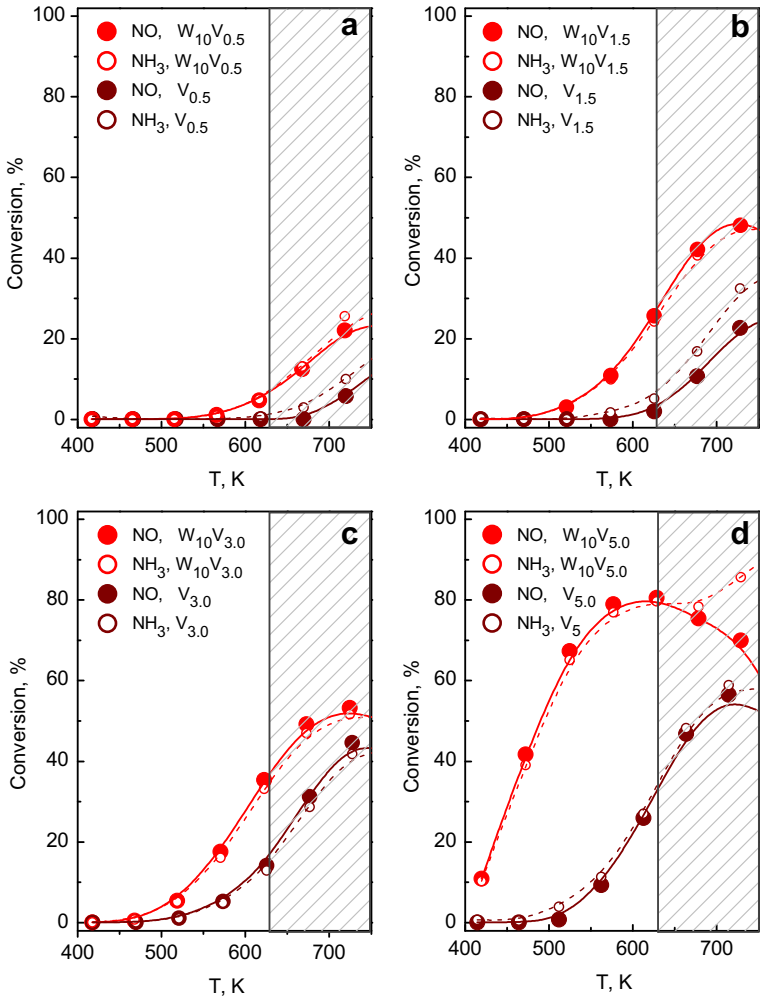

Fig. 2. NO and NH_3 conversions during the SCR of NO with ammonia over the V_2O_5/TiO_2 and V_2O_5—WO_3/TiO_2 catalysts used in this study. 1000 ppm NO, 1000 ppm NH_3, and 2% O_2 in He, GHSV = 750,000 h^{-1}.

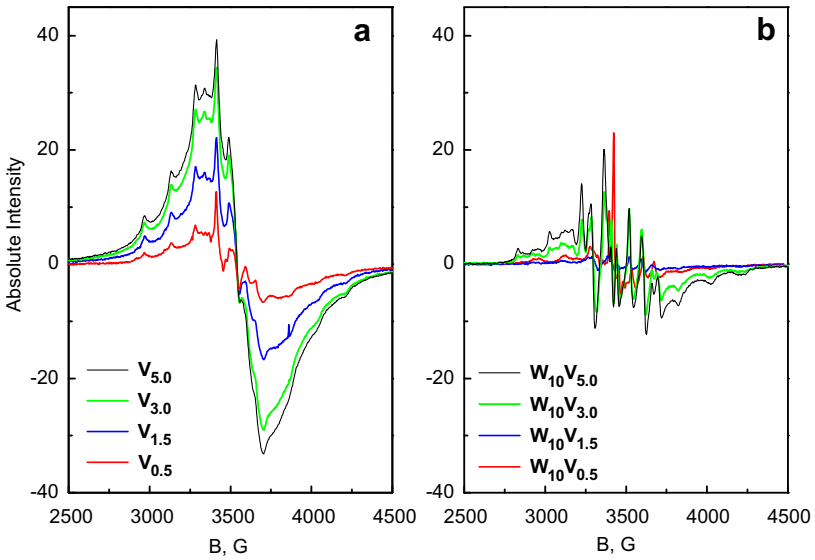

Fig. 3. EPR spectra of tungsten-free and tungsten-containing V_2O_5/TiO_2 catalysts after the reference calcination (623 K, 1 h), measured at 77 K. (For interpretation of the references to colour in this figure, the reader is referred to the web version of this article.)

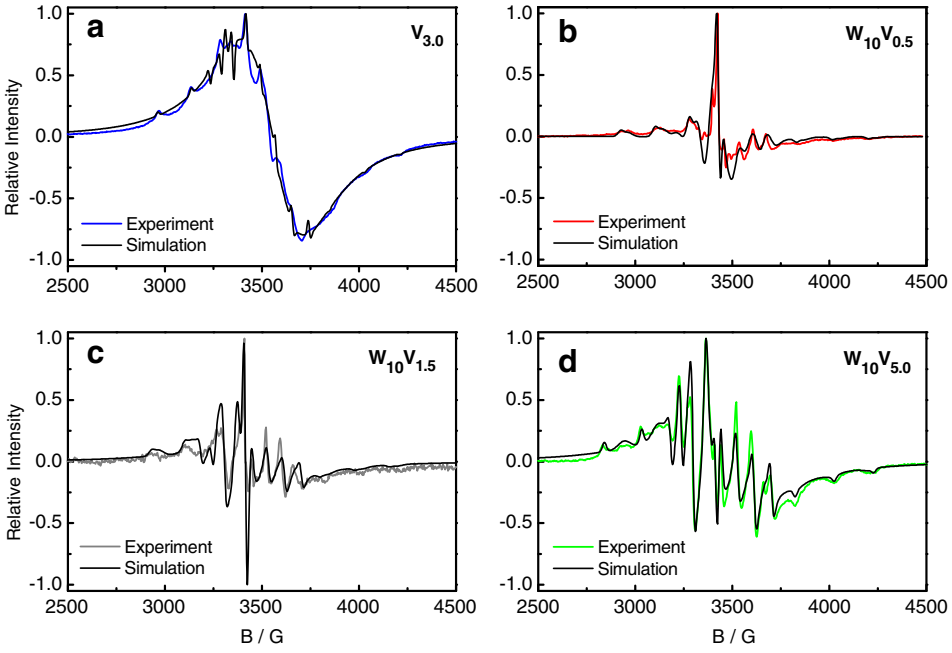

Fig. 4. Examples for the simulation of the EPR spectra of tungsten-free and tungsten-containing V_2O_5/TiO_2 catalysts (cf. Fig. 4).

Examples for the quality of the simulation are given in Fig. 4. While a better coincidence between experimental and simulated signals would have been desirable in particular for the tungsten-free catalysts (cf. Fig. 4a, central part between 3250 and 3350 G), the major features are apparently reproduced by the model. Most of the divergences can be traced back to a limitation of the software which does not allow using different line widths for the individual hyperfine lines, although variations are obvious. In the V multiplets, the positions of the outermost $A_{||}$ hyperfine lines at low and high field are well fitted in all cases which suggests that the number of superimposed signals and, thus, of different single VO^{2+} sites, and their basic parameters (g and A values) are basically correct.

In absence of tungsten, the hyperfine structure signal of isolated VO^{2+} could be fitted with almost identical parameters in all samples (Table 2, species 1). Both axial distortion ($\Delta g_{||}/\Delta g_{\perp} = 2.15$) and degree of delocalization ($\beta_2^{*2} = 0.56$) do not depend on the vanadia loading. At low vanadium content, a second hfs signal can be observed, but it could be simulated only for $V_{0.5}$ (Table 2, species 2). This VO^{2+} species has a slightly lower axial distortion ($\Delta g_{||}/\Delta g_{\perp} = 1.96$), and the unpaired electron is closer to the V^{4+} center ($\beta_2^{*2} = 0.77$). However, compared to the signal of the clustered phase, the hfs signals are minor. In $V_{0.5}$, the isotropic signal is ≈50 times more intense than the latter, and its predominance increases with the vanadium content: in V_5 the intensity ratio (I_{rel}) is as large as 340, although the theoretical coverage of the surface V oxide species is on the order of only 0.2.

In the spectra of the tungsten-containing samples, two signals of isolated VO^{2+} species were always found (Fig. 3b, Fig. 4b–d, Table 3). The spectral parameters of these signals are different from

Table 2
Simulated parameters of the EPR spectra of V_2O_5/TiO_2 catalysts (cf. Fig. 3a, Fig. 4a) and parameters calculated thereof. g and A values, relative intensities [a] (I_{rel}), $\Delta g_{||}/\Delta g_{\perp}$ (axial distortion of VO^{2+} site) and delocalization coefficient β_2^{*2} (see text).

	Species	$g_{||}$	$g_{\perp}$	$A_{||}$	$A_{\perp}$	$I_{rel.}$[a]	$\Delta g_{||}/\Delta g_{\perp}$	β_2^{*2}
$V_{0.5}$	1	1.905	1.957	176 G	73 G	1	2.15	0.56
	2	1.933	1.967	173 G	63 G	0,7	1.96	0.77
	Singlet	1.924		–		79 {53}[b]	–	–
$V_{1.5}$	1	1.905	1.957	179 G	73 G	1	2.15	0.56
	Singlet	1.924		–		185	–	–
$V_{3.0}$	1	1.905	1.957	179 G	73 G	1	2.15	0.56
	Singlet	1.924		–		261	–	–
$V_{5.0}$	1	1.905	1.957	179 G	73 G	1	2.15	0.56
	Singlet	1.924		–		340	–	–
[41]	1	1.925	1.982	199	72		3.77	0.72
	2	1.939	1.975	182	58		2.30	0.72
[50]	1	1.93	1.978	199	78		2.97	0.69
	2	1.94	1.963	170	57		1.59	0.66

[a] Intensity of singlet signal related to signal 1.
[b] Related to sum of isolated sites.

those in absence of vanadium; therefore they have been labeled species 3 and 4, although their properties vary with the V content unlike those of the major species in absence of tungsten. The variation concerns, in particular, the degree of axial distortion ($\Delta g_{||}/\Delta g_{\perp}$ of species 3 ranging from 2.36 at 0.5 wt.% V_2O_5 to 3.2–3.3 at 3–5 wt.% V_2O_5, species 4 from 2.85 at 0.5 wt.% V_2O_5 to 4.83 5 wt.% V_2O_5), while the location of the unpaired electron is rather similar in all cases and closer to V than in absence of tungsten ($\beta_2^{*2} = 0.81 - 0.88$). Species 4 is apparently more strongly distorted than species 3. There is also a broad isotropic signal in presence of tungsten. Notably, its intensity ratio to the hfs signals is much smaller than in absence of tungsten. It increases very moderately with the vanadium content, just doubling from 5 to 10 at a tenfold increase of the vanadium loading.

3.3.2. Temperature-programmed reduction

In Fig. 5, TPR profiles of reference samples are compared with those of some catalysts in order to derive an assignment for the features observed. The hydrogen consumption data are summarized in Table 4. The TiO_2 hydrate gave a reduction signal between 630 and 850 K, which can be assigned to the reduction of the sulfate species to SO_2. It comprises three sub-signals at 643 K, 753 K, and 813 K which indicates a strong heterogeneity of the surface sulfate species [43]. The hydrogen consumption (Table 4) is well in agreement with a sulfate content of ≈2 wt. In the V_2O_5/TiO_2 catalysts, the sulfate was co-reduced with the vanadium at lower temperatures (see $V_{1.5}$ in Fig. 5, with a peak temperature of 740 K, and Fig. 6a). Tungsten oxide supported on the TiO_2 hydrate was reduced in two steps (Fig. 5, W_{10}). The hydrogen consumption data confirm that the first step at 860 K originates from the reduction of W(VI) to W(IV), which is reduced to W(0) in the second peak around 1160 K. In presence of vanadium ($W_{10}V_{1.5}$), there are indeed three signals, but with unexpected relation of the hydrogen consumption. The W(VI) → W(IV) reduction peak is much smaller than in W_{10}, whereas the signal for vanadia reduction is large. This suggests that tungsten ions in the vicinity of surface vanadium oxide species are coreduced with the latter and only non-interacting surface tungsten oxide species show up at ≈860 K.

The TPR profiles of all catalysts are displayed in Fig. 6. In absence of tungsten, the vanadium was always reduced in one step, which superimposes the sulfate reduction. With growing vanadia content, the peak temperature decreased from 800 K ($V_{0.5}$) to 720 K ($V_{5.0}$). $V_{5.0}^{*}$ reduced in a somewhat broader single peak centered at 745 K (not shown). The hydrogen consumptions indicate a reduction of V(V) to V(III), the remaining consumption agreeing roughly with the reduction of ca. 2 wt.% sulfate (Table 4). In presence of tungsten, the three-peak pattern discussed above can be seen in all cases (Fig. 6b). The central peak representative for surface tungstate not interacting with surface vanadate was always smaller than in vanadium-free W_{10} (light-gray trace at the bottom of the diagram). The signals have been fitted with Gaussian lines to estimate the H_2 consumptions for the individual species, and the results are given in Table 4. The accuracy of these data is limited because possible increases of the baseline at high temperatures (cf. Fig. 6a) would have exaggerated the values for the high-temperature signal. However, it is clear that the hydrogen consumption of the 860 K signal is always smaller than expected, and the consumption in the first signal significantly exceeds the sum of consumptions due to sulfate and vanadium reduction. The latter difference may be even underestimated because the total H_2 consumption measured was always short of the expected value (sum of consumptions for V, W, and sulfate species), and there was no sulfate peak discernible in the profile of W_{10} (Fig. 5). Probably, the intermediate calcination of the tungsten-containing support at 713 K had resulted in a significant loss of sulfate, therefore the

Table 3
Simulated parameters of the EPR spectra of V_2O_5—WO_3/TiO_2 catalysts (cf. Fig. 3b, Fig. 4b–d) and parameters calculated thereof. g and A values, relative intensities[a] (I_{rel}), $\Delta g_{||}/\Delta g_{\perp}$ (axial distortion of VO^{2+} site) and delocalization coefficient β_2^{*2} (see text).

	Species	$g_{||}$	$g_{\perp}$	$A_{||}$	$A_{\perp}$	$I_{rel.}$	$\Delta g_{||}/\Delta g_{\perp}$	β_2^{*2}
$W_{10}V_{0.5}$	3	1.919	1.967	182 G	67 G	1.0	2.36	0.81
	4	1.899	1.966	183 G	60 G	1.6	2.85	0.88
	Singlet	1.976		–		14 {5.4}[b]	–	–
	O_2^- (Ti)	1.995		–		0.06	–	–
$W_{10}V_{1.5}$	3	1.917	1.975	182 G	57 G	1.0	3.12	0.88
	4	1.925	1.980	187 G	65 G	0.16	3.47	0.85
	Singlet	1.968		–		8 {6.0}[b]	–	–
	O_2^- (Ti)	2.003		–		0.03	–	–
$W_{10}V_{3.0}$	3	1.934	1.982	198 G	79 G	1.0	3.30	0.86
	4	1.914	1.981	180 G	67 G	2.0	4.17	0.81
	Singlet	1.976		–		26 {8.7}[b]	–	–
	O_2^- (Ti)	2.003		–		0.03	–	–
$W_{10}V_{5.0}$	3	1.934	1.981	198 G	73 G	1.0	3.21	0.86
	4	1.914	1.984	180 G	69 G	1.7	4.83	0.80
	Singlet	1.976		–		28 {10.4}[b]	–	–
	O_2^- (Ti)	2.003		–		0.02	–	–

[a] Intensity of singlet signal related to signal 3.
[b] Related to sum of isolated sites.

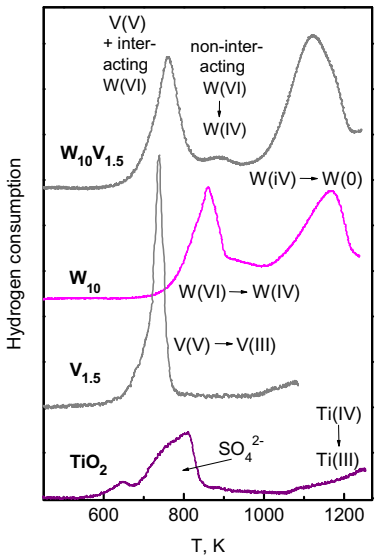

Fig. 5. Temperature-programmed reduction of titania hydrate support, bare and loaded with V_2O_5 (1.5 wt.%), WO_3 (10 wt.%) or both V_2O_5 (1.5 wt.%) and WO_3 (10 wt.%). Temperature ramp – 10 K min^{-1}.

excess consumption during V(V) reduction is most likely larger than suggested by the figures in Table 4.

The profiles of the samples with high vanadium content exhibit another remarkable feature – a sharp peak preceding the top of the signal assigned to coreduction of interacting surface vanadium and tungsten oxide species. The peak shape is reminiscent of the signal shapes obtained in absence of tungsten (Fig. 6a). This suggests that the narrow tip may originate from separate surface vanadium oxide species, which are not influenced by surface tungstates. At 1.5 wt.% V_2O_5 and below, such narrow signal was not observed. On the basis of the proposed assignment, this would mean that practically all of the surface vanadate species are in the vicinity of surface tungstate species, only at higher vanadium content, a significant amount of surface vanadium oxide islands or clusters is present.

3.4. Raman spectroscopy

Raman spectroscopy is the method that has provided most information on the speciation of vanadium sites in supported vanadium oxide catalysts so far. FT-Raman spectra of the initial titania hydrate and of an anatase and a rutile reference are presented in Fig. 7a, whereas the spectra of the catalysts $V_{1.5}$, $W_{10}V_{1.5}$, $V_{5.0}$, and $W_{10}V_{5.0}$ are depicted in Fig. 7b. In the bare support (Fig. 7a), the signal position of all lines agree very well with those of the reference anatase, although the lines are significantly broader. The latter explains why the overtone of the 395 cm^{-1} vibration at 796 cm^{-1} is not resolved. Although the anatase structure can be clearly identified for the support, differences in the intensity distribution between the major signals at 638 cm^{-1}, 515 cm^{-1}, and 395 cm^{-1} should be noted. In particular, the E_g vibrations [44] (638 cm^{-1}, also 197 cm^{-1} and 150 cm^{-1}, which are cut off in Fig. 7) are less distinct in the titania hydrate than in the reference anatase.

Surprisingly, no signals for surface vanadium or tungsten oxide species could be found in the spectrum of $W_{10}V_{1.5}$ (Fig. 7b). The intensity distribution between the major bands at 638 cm^{-1}, 515 cm^{-1}, and 395 cm^{-1} was slightly changed, with a somewhat higher intensity at 638 cm^{-1}, but there was no signal between 800 and 1100 cm^{-1} except for the very weak overtone at ca. 800 cm^{-1}. Fig. 7b contains also a spectrum measured with the same catalyst after a thermal treatment (873 K, 4 h) which brought the BET surface down to 71 m^2/g. Here, a signal of the supported species is clearly discernible. In Fig. 7a, a spectrum of the TiO_2 hydrate calcined to bring its BET surface area down to 128 m^2/g (673 K, 1 h) is presented as well. The shifts in the intensity distribution of the anatase bands are very similar to those in $W_{10}V_{1.5}$.

With the highest vanadium oxide content, it was possible to detect signals of the supported species even after the reference calcination. In $V_{5.0}$, a signal at 1026 cm^{-1} can be clearly discerned. When 5 wt.% V_2O_5 were supported on the precalcined TiO_2 ($V^*_{5.0}$), the signal became broad, extending to wave numbers below 1000 cm^{-1}, although there was still intensity around 1030 cm^{-1}. The spectrum of $W_{10}V_{5.0}$ was almost identical with that of $V^*_{5.0}$.

No signals of surface tungsten oxide species could be observed on a vanadium-free catalyst (W_{10}) which was calcined to achieve a BET surface area of ca. 80 m^2/g (not shown).

4. Discussion

4.1. Catalytic properties

The catalysts prepared and investigated in the present study are related to technical SCR catalysts only with respect to their composition and to the relatively simple preparation technique. As the

Table 4
Hydrogen consumptions in the TPR experiments. Comparison of measured with expected values[a].

Sample	H_2 consumption, mmol/g	V(V) → V(III) mmol/g, expected	W(VI) → W(0) mmol/g, expected	SO_4^{2-} → SO_2 mmol/g, calculated[b]
TiO_2	0.24	–	–	0.24
W_{10}	1.19	–	1.29	–
$V_{0.5}$	0.31	0.05_5	–	0.25_5
$V_{1.5}$	0.35	0.16_5	–	0.18_5
$V_{3.0}$	0.57	0.33	–	0.24
$V_{5.0}$	0.80	0.55	–	0.25

	H_2 consumption up to [...] K mmol/g	V(V) → V(III) + sulfate reduction, mmol/g		W(VI) → W(IV), mmol/g	
		Expected[c]	Measured	Expected	Measured
W_{10}	[1000 K] 0.40			0.43	0.40
$W_{10}V_{0.5}$	[980 K] 0.55	0.31	0.38	0.43	0.17
$W_{10}V_{1.5}$	[980 K] 0.70	0.35	0.49	0.43	0.21
$W_{10}V_{3.0}$	[970 K] 0.81	0.57	0.64	0.43	0.17
$W_{10}V_{5.0}$	[940 K] 1.07	0.80	0.98	0.43	0.09

[a] Accuracy in presence of W limited due to unclear course of baseline.
[b] Difference between real consumption and expectations for V and W reduction; 2 wt.% sulfate ≅0.21 mmol/g,
[c] Sum of H_2 consumptions for V(V) and sulfate reduction of tungsten-free catalysts.

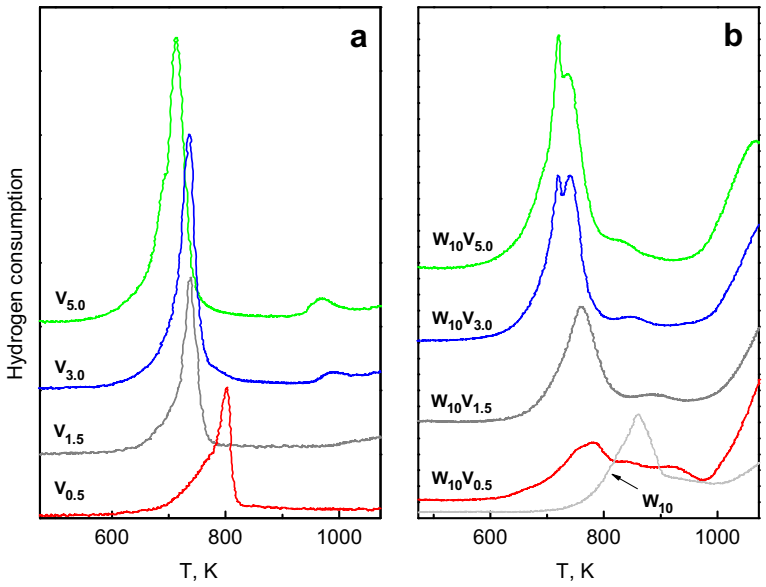

Fig. 6. TPR profiles of tungsten-free and tungsten-containing V_2O_5/TiO_2 catalysts. In (b), the profile of 10% WO_3/TiO_2 from Fig. 5 is repeated for comparison.

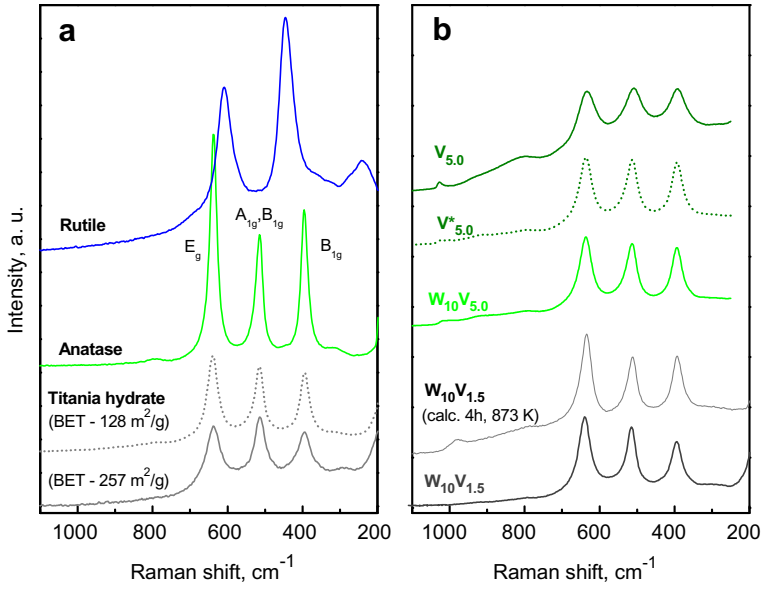

Fig. 7. FT-Raman spectra of reference compound (a) and of selected V_2O_5(—WO_3)/TiO_2 catalysts after reference calcination (623 K, 1 h, b). References – anatase and rutile, both Sachtleben Chemie GmbH, Germany. The spectra of $V_{5.0}$, $V^*_{5.0}$, and of $W_{10}V_{5.0}$ were measured with the DRX Raman Microscope (see Section 2.2.).

purpose of the study was to investigate the effect of surface tungstate species on the vanadium oxide speciation, the samples deliberately deviated from technical catalysts: first, in their large BET surface area, because the theoretical transition metal oxide surface coverage was to be kept below 1, and second, in their thermal history. It is known that calcination at high temperatures may improve the activity of V_2O_5—WO_3/TiO_2 catalysts [3]. Here, exposure to $T > 623$ K was avoided to confine solid-state reactions to the fixation of the impregnated transition metal oxide species to the support. The catalytic data obtained with these samples (Fig. 2) show that the typical promotion effect of tungsten was obtained despite these deviations. This holds, in particular, for the boost of activity caused by the tungsten promoter: at identical V_2O_5 content, the NO conversions always increased at significantly lower temperatures in presence of tungsten. Remarkably, this effect is most pronounced at large vanadium contents. The reported widening of the temperature window for the selective NO reduction [2,4,6] cannot be confirmed with the present set of samples as their structure might change above the calcination temperature of 623 K.

4.2. Raman spectra

The study of the structural properties of the supported vanadium and tungsten oxide species by Raman spectroscopy provided less information than expected. No crystalline V or W oxide phases were detected by XRD (Fig. 1), but the direct observation of surface vanadate or tungstate species by Raman spectroscopy [9–11,14] was possible only at the highest vanadium oxide loading. Apparently, the signals seen there were all due to surface V oxide species

because no signals were detected on a tungsten-only catalyst with the spectrometer used. Indeed, it has been reported that the Raman cross sections of supported tungsten oxide species are significantly smaller than that of supported V oxide species [11].

The comparison of spectra taken with $W_{10}V_{1.5}$ after the reference calcination and after thermal treatment at 873 K (Fig. 7b) suggests that the failure to detect the supported V oxide species is not due to insufficient sensitivity of the spectrometer. Instead, we believe it may be due to a strong energetic heterogeneity of the species on the high surface area support. This would cause distortions of the coordination polyhedra and influence the V=O wave numbers resulting in broadening of the corresponding signals [45] up to their disappearance in the background. On the other hand, signals of three-dimensional oxide phases (V_2O_5, WO_3), which are traced by their characteristic bands (V_2O_5 – 994 cm^{-1}, WO_3 – 800 cm^{-1}) with great sensitivity due to the generally large interaction cross sections of the bulk oxide phases [11,46–48], were not found either. Therefore, the expected two-dimensional structure of the surface vanadium and tungsten oxide phase can be supported indirectly at least.

The signal at 1026 cm^{-1} observed in the spectrum of $V_{5.0}$ can be assigned to isolated surface vanadium oxide species [11]. Its broadening toward lower wave number in $V^*_{5.0}$ is difficult to explain because the V=O bonds in surface polyvanadate species, which should be more abundant given the lower surface area of the support, are rather expected at higher wave numbers [49]. One might assume that the broadening is a result of the more intense very broad structure centered around 930 cm^{-1}, which is due to V—O—V vibrations in polyvanadates. Due to the low Raman interaction cross sections of these species, their presence already in $V_{5.0}$ cannot be excluded on the basis of the spectrum in Fig. 7b. In the spectrum measured with the tungsten-containing catalyst ($W_{10}V_{5.0}$), the broadening may also contain intensity from V—O—W structures.

It should be also noted that the spectra of the supported catalysts are still significantly different from that of the reference anatase. In the initial titania hydrate, a defective structure may be assumed, where a distortion of the tetragonal anatase structure has a particular effect on the symmetry of the multidimensional vibrations. Indeed, the discrepancy between particle diameters deduced from nitrogen physisorption and from XRD (section 3.1) suggests the presence of porous, disordered material to which the effect might be ascribed. However, this does not hold for $W_{10}V_{1.5}$ where the BET surface area had decreased by more than 50% and particle dimensions from the BET surface area and the diffractograms were close. The spectrum taken from the bare support calcined down to 128 m^2/g (Fig. 7a) shows that the structural distortions are not induced by the transition metal oxide species loaded on the surface of $W_{10}V_{1.5}$ – which would have been surprising for particles of >10 nm diameter. Instead, we believe that the deviating pattern of Raman intensities arises from an internal defectivity of the TiO_2 particles, which needs temperatures in excess of 713 K (calcination temperature of the WO_3/TiO_2 precursor) to be healed. This defectivity may have contributed to the structural heterogeneity of the surface vanadates and tungstates which has probably impeded their observation in the Raman spectra.

4.3. EPR spectra

In the EPR spectra, V(IV) defects in the fully oxidized catalysts are detected. The relative abundance of these defects has been reported to be in the order of 8–10% in this type of catalyst [6]. However, this relative abundance may be different for each species identified, e.g., for all types of VO^{2+} sites discussed below. Strictly speaking, it may differ even for the (most likely two-dimensional) clusters causing the singlet signals in presence or absence of tungsten because of the differences in the *g* values (Tables 2 and 3). Therefore, the signal intensity ratios reported should not be understood as concentration ratios, and even the trends which will be outlined are not conclusive on their own unless confirmed by an independent method. This confirmation was obtained by the TPR results (*vide infra*).

The most striking feature of the EPR study is the pronounced difference in the clustering (*viz.*, island formation) tendency of the surface vanadium oxide species in presence or absence of tungsten (Fig. 3). Without tungsten, a strong isotropic singlet of interacting V(IV) ions was obtained already at a theoretical surface coverage of just 2–3% ($V_{0.5}$). The further increase of the intensity ratio between this singlet and the isolated V sites with growing vanadium content (Table 2) is no surprise on this background. In the presence of tungsten, the singlet signal is much smaller, actually hardly to be seen on the same intensity scale up to 1.5 wt.% V_2O_5 (Fig. 3b), and despite the mentioned risks due to possible different defect formation tendencies, the conclusion that tungsten suppresses island formation of the surface vanadium oxide species appears quite plausible. This may be due to an affinity of surface tungsten and vanadium oxide sites to interact with each other for energetic reasons, or it may be a consequence of the tendency of surface tungstates to form isolated sites even at high coverage [11], which would leave limited space for island formation from a second component.

In absence of tungsten, up to two signals of isolated vanadium oxide sites were identified on top of the singlet signal. In the literature, similar signals were assigned to VO^{2+} interacting with TiO_2 alone or with sulfate and TiO_2 [41,50]. In our study, signal (2) was observed only at 0.5 and 1.5 wt.% V_2O_5, too weak for reliable simulation in the latter case. This suggests its assignment to the sulfate-related site, because the concentration of sulfate is fixed and the abundance of isolated vanadium oxide sites interacting with it should decrease as these sites would be more and more included into islands. Indeed, there is fair agreement between the spectral parameters of this signal and the corresponding signals assigned to sulfate-related VO^{2+} by other authors (Table 2, signals labeled "2"). Signal 1 arises, therefore, from VO^{2+} sites interacting with the TiO_2 surface only. Here, the considerable deviation of the spectral parameters from those reported in the literature (Table 2) is surprising. This divergence might be assigned to difference in surface properties of the anatase supports. The better coincidence of the spectral parameters of the sulfate-related VO^{2+} may indicate that the properties of this site are dominated by the interaction with the sulfate species.

In the presence of tungsten, two signals of isolated VO^{2+} species were observed, which differed from those found in absence of tungsten not only by their spectral parameters, but also by the dependence of the latter on the vanadium content (Table 3). Given the deviations in the spectral parameters of VO^{2+} on different anatase supports, the moderate difference in the properties of signal 1 and signal 3 (in $W_{10}V_{0.5}$) would not suffice to conclude an influence of tungsten on the latter, but the continuous increase of the axial distortion ($\Delta g_{||}/\Delta g_{\perp}$) with the vanadium content both in signal 3 and 4 strongly suggests such interaction. Both signals apparently reflect a certain average number of tungsten atoms around the vanadium site. As it is unlikely that the distribution of such "coordination numbers" would be bimodal in all samples, there must be another difference causing the presence of two well-defined signals in all cases. A tentative explanation might be the vicinity of isolated vanadate and tungstate sites reflected in signal 3, whereas signal 4 might arise from species involving (an) oxygen bridge(s) (V—O—W) between them.

The above-mentioned increase of the axial distortion may indicate a growing interaction of the isolated vanadium site with tungstate neighbors, which is not *á priori* plausible at decreasing W/V ratio. A tentative explanation would rely on the tendency of surface vanadate and tungstate species to interact with each other

(*vide supra*), enhanced by the decreasing availability of free surface area. In Fig. 3b, it can be observed that the singlet signal did not show a continuous increase with the vanadium content but was smallest in $W_{10}V_{1.5}$. At a surface coverage of 0.6...0.8 ($W_{10}V_{0.5}$, see Table 1), there seems to be sufficient space to form some surface vanadium oxide islands even in presence of the surface tungstate phase. However, the spectroscopic difference of the isolated sites (in particular site 4) from those found in absence of tungsten (Tables 2 and 3) indicates that pairing between surface vanadium and tungsten oxide species already competes with island formation. With decreasing available space, the vanadium islands would be first consumed by the W—V pairing tendency and then reappear, maybe in smaller size, due to the abundance of vanadium oxide species to be accommodated at the highest vanadium contents. The very low intensity of these singlet signals as compared to those of the tungsten-free samples (Fig. 3) may suggest that a relatively small part of the vanadium is engaged in the islands. Hence, a large quantity of vanadium has to be separated by the tungsten present in particular at the higher vanadium contents. At W/V ratios approaching equimolarity, this will lead to a well-mixed surface oxide phase. As free space is less and less available with increasing transition metal oxide loading, the vanadium oxide sites will have to be surrounded more and more completely by tungstate species to avoid island formation, which might explain the increased distortion of the isolated V sites.

4.4. Temperature-programmed reduction

The TPR profiles confirm this model to a large extent. V_2O_5—WO_3/TiO_2 catalysts were subjected to temperature-programmed reduction earlier [43,51], and the basic patterns observed in our study were known before. An excess of the hydrogen consumption over the expectations for V(V) reduction was noted by Reiche et al. in their report on the V_2O_5—WO_3/TiO_2 Eurocat round robin [51], and shoulders at the low- and high-temperature side of the first peak were mentioned. On the Eurocat, the first peak appeared at significantly higher temperature than in our case (845 K vs. 735–780 K), although the temperature region of the high-temperature peak was similar (1140 K vs. >1100 K except for $W_{10}V_{5.0}$, peaks are cut off in Fig. 6b). The larger intermediate temperature range in our case may have favored the detection of the weak signals assigned to surface tungsten oxide species not in interaction with vanadia.

To the best of our knowledge, the observation of this signal and also of a sharp tip at the low-temperature signals at higher vanadium content (Fig. 6b) assignable to surface vanadia islands is new. It permits assigning the excess H_2 consumption of the first peak to W(VI) species interacting with surface vanadia species. Although the quantitative evaluation of component signals in the interval between the two main peaks is not very accurate, the data suggest that ever more surface tungsten oxide species interact with the vanadium oxide with increasing V content. On the other hand, nearly all surface vanadate species are in interaction with tungsten oxide sites at low vanadium content, whereas at high vanadia loadings, some island formation is indicated by the TPR profiles, in good agreement with the conclusions from EPR.

4.5. Consequences for the promoting influence of tungsten in V_2O_5—WO_3/TiO_2 catalysts

The observations made in this study are at variance with the view that the promoting effect of tungsten in V_2O_5—WO_3/TiO_2 SCR catalysts can be explained by a mere compression of the surface vanadate phase by the competition for the support surface, which would induce formation of highly active V—O—V paired structures from less active isolated vanadium oxide sites. In particular, our EPR study shows that the extent of (two-dimensional) clustering is much larger in tungsten-free catalysts, it is instead reduced by the introduction of tungsten. When such disruption of surface vanadia islands causes sizeable increases of the catalytic activity, a different explanation for the promotional effect has to be found.

The isolated sites detected by EPR might be seen as candidates for the explanation of this effect. On the basis of the present data, such hypothesis cannot be appropriately examined as the introduction of tungsten most likely changes two parameters at the same time – the abundance and the structure of the sites (cf. spectral parameters in Tables 2 and 3). From an investigation of thermal treatments with $W_{10}V_{1.5}$, which will be reported in a future pair of papers [37,52], we can, however, exclude all species detectable by EPR (including the singlet signal) from being relevant for the catalytic activity because catalyst states with very different catalytic behavior were found to provide identical EPR spectra. This is not really surprising because the binuclear V—O—V sites favored by most groups cannot be singled out in our spectra: they might contribute to the singlet, where they are heavily superimposed by signals from larger entities, or they might produce a signal with different axial distortion (V(IV)—O—V(V) bound to the support), which would be enhanced with the vanadium content. This was, however, not observed.

Our interpretation is therefore that the promotion effect of tungsten is just related to its ability to prevent excessive V_xO_y island formation and to create a mixed surface phase with small surface vanadium and tungsten oxide entities. Among these entities, the isolated sites can be detected by EPR, but one can expect that the structure created contains binary sites as well, maybe trimers and other oligomers of low nuclearity. As a grave influence of three-dimensional clustering may be ruled out for our catalysts, samples with identical vanadium content will expose the same number of vanadium sites – once predominantly in more or less extended islands (V_2O_5/TiO_2), once predominantly in isolated sites and small oligomers with tungstate neighbors (V_2O_5—WO_3/TiO_2). The significantly larger activity of the latter may be due to a specific influence of the tungstate species on the nearby vanadate sites or to a superior activity of binuclear V—O—V sites (or small oligomers) compared with V—O—V entities in extended islands. A decision between these choices cannot be made on the basis of the evidence presented so far. Results of the above-mentioned study about the effect of thermal stress on $W_{10}V_{1.5}$, which will be published in the future [37,52], will provide some evidence in favor of the second explanation.

5. Conclusions

By studying V_2O_5/TiO_2 catalysts of varying V_2O_5 content with and without 10 wt.% WO_3 by electron-paramagnetic resonance and temperature-programmed reduction, it has been found that the structure of the surface vanadium oxide species is strongly perturbed in presence of surface tungstate species. In absence of WO_3, the surface vanadates exhibit a pronounced tendency to island formation, which is strongly suppressed in presence of tungsten. From the TPR profiles, it may be suggested that most of the surface tungstate species are surrounded by surface vanadates and vice versa, i.e., a well-mixed surface oxide phase is formed instead of a system of coexisting islands. Explanations for the promoting effect of tungsten should be sought in the intimate mixing between the transition metal oxide species rather than in a compression of the surface vanadate phase by the coexisting surface tungstate phase. They may include specific effects of the tungstate species on neighboring vanadium sites or a superior activity of small (dimeric, oligomeric) vanadium sites as compared to sites in extended islands.

Acknowledgments

We acknowledge gratefully experimental support by Dr. Jennifer Strunk (FT-Raman spectroscopy), Dr. T. Reinecke (XRD), and Ms. Inga Ellmers and Rosemary Fowler (Catalysis), and fruitful discussions on problems related to Raman spectroscopy with Dr. Gerhard Mestl (Süd-Chemie AG).

References

[1] H. Bosch, F.J.J.G. Janssen, Catal. Today 2 (1988) 369–531.
[2] L. Lietti, P. Forzatti, F. Bregani, Ind. Eng. Chem. 35 (1996) 3884–3892.
[3] G. Madia, M. Elsener, M. Koebel, F. Raimondi, A. Wokaun, Appl. Catal. B 39 (2002) 181–190.
[4] J.P. Chen, R.T. Yang, Appl. Catal. A 80 (1992) 135–148.
[5] G. Oliveri, G. Ramis, G. Busca, V.S. Escribano, J. Mater. Chem. 3 (1993) 1239–1249.
[6] L.J. Alemany, L. Lietti, N. Ferlazzo, P. Forzatti, G. Busca, E. Giamello, F. Bregani, J. Catal. 155 (1995) 117–130.
[7] G. Ramis, G. Busca, C. Cristiani, L. Lietti, P. Forzatti, F. Bregani, Langmuir 119 (1992) 1744–1749.
[8] W. Weisweiler, Chem. Eng. Technol. 72 (2000) 441–449.
[9] I.E. Wachs, J. Catal. 124 (1990) 570–573.
[10] G.T. Went, S.T. Oyama, A.T. Bell, J. Phys. Chem. 94 (1990) 4240–4246.
[11] M.A. Vuurman, I.E. Wachs, A.M. Hirt, J. Phys. Chem. 95 (1991) 9928–9937.
[12] H. Eckert, I.E. Wachs, J. Phys. Chem. 93 (1989) 6796–6805.
[13] G.T. Went, L.J. Leu, A.T. Bell, J. Catal. 134 (1992) 479–491.
[14] G.C. Bond, Appl. Catal. A 157 (1997) 91–103.
[15] H.J. Tian, E.I. Ross, I.E. Wachs, J. Phys. Chem. B 110 (2006) 9593–9600.
[16] M.A. Banares, I.E. Wachs, J. Raman Spectrosc. 33 (2002) 359–380.
[17] L.E. Briand, O.P. Tkachenko, M. Guraya, X. Gao, I.E. Wachs, W. Grünert, J. Phys. Chem. B 108 (2004) 4823–4830.
[18] M. Inomata, A. Miyamoto, Y. Murakami, J. Catal. 62 (1980) 140–148.
[19] L. Lietti, P. Forzatti, Appl. Catal. B 3 (1993) 13–35.
[20] F.J.J.G. Janssen, F. van den Kerkhof, H. Bosch, J. Ross, J. Phys. Chem. 91 (1987) 5921–5927.
[21] F.J.J.G. Janssen, F. van den Kerkhof, H. Bosch, J. Ross, J. Phys. Chem. 91 (1987) 6633–6638.
[22] G.T. Went, L.J. Leu, R.R. Rosin, A.T. Bell, J. Catal. 134 (1992) 492–505.
[23] M.D. Amiridis, I.E. Wachs, G. Deo, J.-M. Jehng, D.J. Kim, J. Catal. 161 (1996) 247–253.
[24] I.E. Wachs, G. Deo, B.M. Weckhuysen, A. Andreini, M.A. Vuurman, M. de Boer, M.D. Amiridis, J. Catal. 161 (1996) 211–221.
[25] U.S. Ozkan, Y.P. Cai, M.W. Kumthekar, J. Catal. 149 (1994) 390–403.
[26] M. Gasior, J. Haber, T. Machej, T. Czeppe, J. Mol. Catal. 43 (1988) 359–369.
[27] N.-Y. Topsoe, H. Topsoe, Catal. Today 9 (1991) 77–82.
[28] N.-Y. Topsoe, J.A. Dumesic, H. Topsoe, J. Catal. 151 (1995) 241–252.
[29] N.-Y. Topsoe, H. Topsoe, J.A. Dumesic, J. Catal. 151 (1995) 226–240.
[30] N.-Y. Topsoe, Science 265 (1994) 1217–1219.
[31] J.A. Dumesic, N.-Y. Topsoe, H. Topsoe, Y. Chen, T. Slabiak, J. Catal. 163 (1996) 409–417.
[32] E. Broclawik, A. Gora, M. Najbar, J. Mol. Catal. A 166 (2001) 31–38.
[33] C. Cristiani, M. Belotto, P. Forzatti, F. Bregani, J. Mater. Res. 8 (1993) 2019–2025.
[34] J.W. Choung, I.S. Nam, S.W. Ham, Catal. Today 111 (2006) 242–247.
[35] G.P. Lozos, B.M. Hofmann, G.C. Franz, Quantum Chemistry Program Exchange, No. 265, 1973.
[36] P.G.W.A. Kompio, PhD Thesis, Bochum, 2010.
[37] P.G.W.A. Kompio, M. Schwidder, G. Hipler, G. Auer, E. Löffler, W. Grünert, J. Catal. submitted for publication.
[38] J.P. Dunn, H.G. Stenger Jr., I.E. Wachs, J. Catal. 181 (1999) 233–243.
[39] K. Bourikas, C. Fountzoula, C. Kordulis, App. Catal. B 52 (2004).
[40] K. Nowinska, A.B. Wieckowski, Z. Phys. Chem. N. F. 62 (1989) 231–234.
[41] A. Brückner, U. Bentrup, J.-B. Stelzer, Z. Anorg. Allg. Chemie 631 (2005) 60–66.
[42] L.J. Boucher, E.C. Tynan, T.F. Yen, Electron Spin Resonance of Metal Complexes, Plenum Press, New York, 1969. p. 111.
[43] S.M. Jung, P. Grange, Appl. Catal. B 21 (2001) 123–131.
[44] T. Ohsaka, F. Izumi, Y. Fujiki, J. Raman Spectrosc. 7 (1978) 321–324.
[45] H. Jeziorowski, H. Knözinger, J. Phys. Chem. 83 (1979) 1166–1173.
[46] S.B. Xie, E. Iglesia, A.T. Bell, Langmuir 16 (2000).
[47] S.S. Chan, I.E. Wachs, L.L. Murrell, J. Catal. 90 (1984) 150–155.
[48] J.P. Baltrus, L.E. Makovsky, J.M. Stencel, D.M. Hercules, Anal. Chem. 57 (1985) 2500–2503.
[49] I.E. Wachs, C.A. Roberts, Chem. Soc. Rev. 39 (2010) 5002–5017.
[50] V. Luca, S. Thomson, R.F. Howe, J. Chem. Soc., Faraday Trans. 93 (1997) 2195–2202.
[51] M. Reiche, M. Maciejewski, A. Baiker, Catal. Today 67 (2000) 347–355.
[52] P.G.W.A. Kompio, A. Brückner, G. Hipler, G. Auer, G. Mestl, E. Löffler, W. Grünert, J. Catal. submitted for publication.